Inhibition of mitochondrial complex I leading to NAD$^+$/NADH imbalance in type 2 diabetic patients who developed late stent thrombosis: Evidence from an integrative analysis of platelet bioenergetics and metabolomics

Mi-jie Gao [a], Ning-hua Cui [b], Xia'nan Liu [a], Xue-bin Wang [a],[*]

[a] *Department of Clinical Laboratory, Key Clinical Laboratory of Henan Province, The First Affiliated Hospital of Zhengzhou University, Zhengzhou, 450000, Henan, China*
[b] *Zhengzhou Key Laboratory of Children's Infection and Immunity, Children's Hospital Affiliated to Zhengzhou University, Zhengzhou, 450000, Henan, China*

A B S T R A C T

Type 2 diabetes mellitus (T2DM) is a strong indicator of late stent thrombosis (LST). Platelet bioenergetic dysfunction, although critical to the pathogenesis of diabetic macrovascular complications, remains uncharacterized in T2DM patients who developed LST. Here, we explored the mechanistic link between the alterations in platelet bioenergetics and LST in the setting of T2DM. Platelet bioenergetics, metabolomics, and their inter-actomes were analyzed in a nested case-control study including 15 T2DM patients who developed LST and 15 matched T2DM patients who did not develop LST (non-LST). Overall, we identified a bioenergetic alteration in T2DM patients with LST characterized by an imbalanced NAD$^+$/NADH redox state resulting from deficient mitochondrial complex I (NADH: ubiquinone oxidoreductase) activity, which led to reduced ATP-linked and maximal mitochondrial respiration, increased glycolytic flux, and platelet hyperactivation compared with non-LST patients. Congruently, platelets from LST patients exhibited downregulation of tricarboxylic acid cycle and NAD$^+$ biosynthetic pathways as well as upregulation of the proximal glycolytic pathway, a metabolomic change that was primarily attributed to compromised mitochondrial respiration rather than increased glycolytic flux as evidenced by the integrative analysis of bioenergetics and metabolomics. Importantly, both bioenergetic and metabolomic aberrancies in LST platelets could be recapitulated ex vivo by exposing the non-LST platelets to a low dose of rotenone, a complex I inhibitor. In contrast, normalization of the NAD$^+$/NADH redox state, either by increasing NAD$^+$ biosynthesis or by inhibiting NAD$^+$ consumption, was able to improve mitochondrial respiration, inhibit mitochondrial oxidant generation, and consequently attenuate platelet aggregation in both LST platelets and non-LST platelets pretreated with low-dose rotenone. These data, for the first time, delineate the specific patterns of bioenergetic and metabolomic alterations for T2DM patients who suffer from LST, and establish the deficiency of complex I-derived NAD$^+$ as a potential pathogenic mechanism in platelet abnormalities.

1. Introduction

Despite successive refinements in stent technologies, stent thrombosis (ST) remains the most severe complication of percutaneous coronary interventions (PCI) with high morbidity (up to 45%) and a high recurrence rate (15–20%) [1]. Recently, multiple registry studies and meta-analyses have reported type 2 diabetes mellitus (T2DM) as a strong predictor for ST, especially for late ST (LST) occurring more than 30 days after implantation [2–4]. Platelet dysfunction, as a hallmark of T2DM [5], may be the potential pathological basis linking T2DM with LST, due to its direct effects on thrombus formation in coronary stents [6].

Platelets, as cytoplasmic fragments of megakaryocytes that contain abundant mitochondria, are considered the most metabolically active organelle, even in the resting state [7]. Upon platelet activation, the cells

need a greater amount of chemical energy, most of which is from the oxidative phosphorylation (OXPHOS) occurring in mitochondria [8]. As mitochondrial impairment progresses during diabetes [9], platelets may initiate a complex sequence of bioenergetic changes involving altered mitochondrial complex activities [10], metabolic switch between OXPHOS and glycolysis [11], and oxidant overproduction [12], all of which may help maintain energy homeostasis but potentially increase platelet sensitivity to thrombotic stimuli [13]. In addition, these bioenergetic changes may also remodel the platelet metabolome, dysregulating the key metabolic pathways controlling platelet activation and aggregation [14]. However, despite the pivotal roles of mitochondrial bioenergetics in platelet function, very little is known about how platelet bioenergetics, including profiles of mitochondrial respiration and glycolysis, contributes to LST, especially in the context of T2DM. Notably, although studies of healthy platelets have suggested significant impacts of bioenergetic changes on the global metabolome [15], the exact role of the bioenergetics-metabolite interactome in platelet thrombotic function and LST risk is still largely unknown.

Herein, using a high-throughput extracellular flux analyzer, we first identified the specific pattern of bioenergetic changes in both the resting and activated states in platelets from T2DM patients who developed LST. Then, by performing untargeted metabolomics in the same population, we uncovered the dysregulated metabolic pathways underlying the bioenergetic aberrancies in LST platelets, and constructed the differential networks of platelet metabolomics and bioenergetics. Finally, we provided ex vivo evidence that the bioenergetic aberrancies observed in LST platelets were at least partially due to inhibition of mitochondrial complex I (CI) and further explored the possibility that targeting mitochondrial respiration by rebalancing the $NAD^+/NADH$ redox state might protect LST platelets against CI inhibition.

2. Materials and methods

2.1. Study population

This was a nested case-control study within a prospective cohort of 1165 type 2 diabetic patients who received primary PCI from September 2017 to September 2019 at the First Affiliated Hospital of Zhengzhou University. The study design of the prospective cohort has been reported previously [16–18]. Briefly, the prospective cohort included subjects who had T2DM but did not suffer from other systemic diseases including cancer, hepatic insufficiency, serious infection, and type 1 diabetes. All participants underwent primary PCI for obstructive coronary artery disease at baseline, and then completed clinical follow-up at 30 days, 1 year, 2 years, and the final follow-up visit (in September 2021) after PCI. During a mean follow-up of 2.5 ± 0.3 years, a total of 15 patients with definite late (>30 days after PCI, n = 9) or very late (>1 year after PCI, n = 6) ST were identified and enrolled in the LST group. Based on the Academic Research Consortium criteria, definite ST was defined as angiographic confirmation of thrombus within the stent with acute onset of ischemic symptoms or ischemic ECG changes or typical rise in cardiac biomarkers [19]. The non-LST group included 15 diabetic patients who did not develop ST and other cardiovascular events (including death, repeated revascularization, myocardial infarction, and stroke) at least 2 years from PCI. LST and non-LST patients were matched on clinical and procedural data at baseline using the propensity score matching method (Table 1). To minimize the influence of antiplatelet therapy on platelet testing, the proportions of non-LST patients on dual antiplatelet therapy (80%, n = 12), aspirin alone (13%, n = 2), and clopidogrel alone (7%, n = 1) were set to exactly match those of the LST patients at the time of platelet isolation. In addition, 15 age- (62.1 ± 7.4 years) and sex-matched (male:female, 9:6) healthy subjects, who had no history of vascular diseases, diabetes, or other systemic diseases and had not used medications known to perturb platelet function in the prior 2 weeks before enrollment [20], were also recruited as healthy controls. Blood collection for platelet isolation was performed at the final follow-up visit

Table 1
Clinical and procedural characteristics of diabetic patients with and without LST.

Variables	LST (n = 15)	Non-LST (n = 15)	P value[a]
Clinical characteristics at baseline			
Age, years	63.7 ± 10.0	64.7 ± 10.1	0.77
Male, n (%)	8 (53.3)	9 (60.0)	1.00
Current smokers, n (%)	6 (40.0)	4 (26.7)	0.70
Body mass index, kg/m^2,	25.6 ± 4.9	26.8 ± 4.9	0.52
Fasting plasma glucose, mmol/L	9.2 ± 2.1	8.6 ± 2.1	0.44
Glycosylated haemoglobin, (%)	7.3 ± 1.4	7.5 ± 1.4	0.64
Diabetes duration, years	9.2 ± 4.2	9.0 ± 4.7	0.88
Diabetes management, n (%)			
Lifestyle modification	2 (13.3)	4 (26.7)	0.76
Oral agents only	4 (26.7)	4 (26.7)	
Insulin only	4 (26.7)	4 (26.7)	
Oral agents and insulin	5 (33.3)	3 (20.0)	
Dyslipidemia, n (%)	4 (27)	2 (13)	0.65
Hypertension, n (%)	5 (33.3)	6 (40.0)	1.00
LVEF <50%, n (%)	5 (33.3)	6 (40.0)	1.00
PCI procedure characteristics			
Clinical Presentations at PCI, n (%)			
Stable angina	3 (20.0)	4 (26.7)	0.90
Unstable angina	1 (6.7)	1 (6.7)	
STEMI	7 (46.6)	5 (33.3)	
USTEMI	4 (26.7)	5 (33.3)	
Stent diameter, mm	3.1 ± 0.4	3.3 ± 0.5	0.29
Stent length, mm	29.3 ± 10.4	31.0 ± 13.5	0.70
Complete revascularization, n (%)	6 (40.0)	8 (53.3)	0.71
Stent type, n (%)			
First generation DES	9 (60.0)	10 (66.7)	1.00
Second generation DES	6 (40.0)	5 (33.3)	
Characteristics at time of LST			
Antiplatelet medications at time of LST, n (%)			
Aspirin only	6 (40.0)		
Clopidogrel only	1 (6.7)		
Aspirin and clopidogrel	8 (53.3)		
Clinical presentations at time of LST, n (%)			
Stable angina	1 (6.7)		
Unstable angina	1 (6.7)		
STEMI	3 (20.0)		
USTEMI	10 (66.6)		
Time from PCI to LST occurrence, days	363 ± 215		
Antiplatelet medications at time of platelet sampling, n (%)			
Aspirin only	2 (13.3)	2 (13.3)	1.00
Clopidogrel only	1 (6.7)	1 (6.7)	
Aspirin and clopidogrel	12 (80.0)	12 (80.0)	

LST indicates late stent thrombosis; LVEF left ventricular ejection fraction; PCI percutaneous coronary interventions; STEMI ST-segment elevation myocardial infarction; NSTEMI non-ST-segment elevation myocardial infarction; DES drug-eluting stent.

[a] Values are mean $\pm$ SD or n (%) as appropriate. P values are obtained from the student *t*-test for continuous variables, and the chi-square test with Yates' correction for categorical variables.

for all participants. The study protocol was approved by the Ethics Committee of the First Affiliated Hospital of Zhengzhou University. All participants gave written informed consent.

2.2. Platelet isolation

Platelet isolation was performed according to the Abcam protocol with minor modifications [20]. Briefly, whole blood samples were collected in citrate by standard venous puncture without a tourniquet to avoid platelet activation [21]. Platelet rich plasma (PRP) was obtained from whole blood by centrifugation (200 *g* for 20 min), diluted 1:1 with HEPES buffer (Gibco, cat# 15630080) containing 1 μM PGE$_1$ (also for preventing platelet activation, Sigma, cat# 900100P), and centrifuged (100 *g* for 20 min) to discard contaminated cell pellets. The obtained platelet rich supernatant was further centrifuged (800 *g* for 20 min) to pellet platelets, which were washed twice with platelet wash buffer

(140 mM NaCl, 3.8 mM $Na_3C_6H_5O_7$, 1 mM EDTA, 1% dextrose). Washed platelets were finally suspended in modified Tyrode's buffer (5 mM HEPES, 5 mM glucose, 140 mM NaCl, 12 mM bicarbonate, 2.6 mM KCl, 0.5 mM $MgCl_2$, pH 7.4) at a density of 1×10^8/mL, unless otherwise stated. Platelet purity was validated by measuring CD41a expression using flow cytometry.

2.3. Ex vivo platelet stimulation

To initiate activation, platelets were treated for 6 min with thrombin (Sigma, cat# T6884), ADP (Sigma, cat# 01905), or collagen (Sigma, cat# 5162). For CI inhibition, non-LST platelets were treated for 30 min with different doses of rotenone (50/100/500 nM, Sigma, cat# R8875). In selected experiments, LST platelets and non-LST platelets pretreated with rotenone were cultured for 30 min with 0.5 μM MitoQ (Abcam, cat# ab285406), 1 mM nicotinamide riboside (NR, MedChemExpress, cat# HY-123033), 20 μM olaparib (MedChemExpress, cat# HY-10162), or 0.1 μM MitoParaquat (MedChemExpress, cat# HY-130278).

2.4. Platelet bioenergetic profiling

Platelet bioenergetics was measured with a Seahorse XFe96 Analyzer (Agilent, Santa Clara, USA). Briefly, suspended platelets (1×10^7 per well) were seeded onto a Seahorse 96-well microplate, centrifuged (700 g, 5 min) to form a monolayer in the well, and maintained in a non-CO_2 incubator at 37 °C for 1 h. Then, based on the protocol of the Mitochondrial Stress Test [22], platelets were sequentially treated with oligomycin (1.0 μg/mL, Abcam, cat# 1404-19-9), FCCP (0.6 μM, Sigma, cat# C2920), and a mixture of rotenone (0.5 μM) and antimycin A (0.5 μM, Sigma, cat# A8674), and the oxygen consumption rate (OCR) was measured over time to calculate the key parameters of mitochondrial respiration involving basal, ATP-linked, proton leak, spare, and maximal respiration (Supplementary Methods). After permeabilization of platelets with the Seahorse Plasma Membrane Permeabilizer (1 nM, Agilent, cat# 102504–100), CI-, II-, and IV-dependent OCRs were measured individually by sequential injections of respiration substrates (Supplementary Methods) [23]. In parallel, the Glycolysis Stress Assay was conducted by sequential treatment of platelets with glucose (19 mM, Sigma, cat# G8270), oligomycin (1 μg/mL), and 2-deoxy-glucose (50 mM, Sigma, cat# D6134), and the extracellular acidification rate (ECAR) was monitored in real time to estimate glycolysis, glycolytic capacity, glycolytic reserve, and non-glycolytic acidification (Supplementary Methods) [24].

2.5. Platelet metabolomic profiling

Details of the metabolomic profiling have been described in our previous reports [25] (also introduced in the Supplementary Methods). Briefly, platelets (3×10^8 per well) were incubated with cold extraction solution (acetonitrile: methanol, 1:1, v/v) containing a mixture of internal standards, and centrifuged (13000 g, 15 min) to remove protein precipitates. The remaining metabolite extracts were further separated using a Vanquish UHPLC system equipped with an UPLC BEH Amide column (2.1 mm × 100 mm, 1.7 μm). Mass spectral detection of the eluted samples was completed on a Q Exactive mass spectrometer (Thermo, Waltham, USA) operated in positive or negative ion mode. The acquired MS raw data were converted to mzXML files, which were uploaded onto the XCMS platform for feature detection and peak alignment [26]. Metabolite annotation was performed by matching the MS2 data of the detected samples to a reference library using the MetDNA webserver [27]. The raw counts for each metabolite were normalized using the best-matched internal standard normalization method [28]. Platelet samples were analyzed in randomized order, with a pooled quality control sample injected at the beginning and end of every 10 samples to qualify instrument performance (Supplementary Fig. 1).

2.6. Platelet aggregation

Light transmittance aggregometry (Chrono-Log Model 700, Havertown, USA) was used to measure platelet aggregation under constant stirring (1000 rpm). Briefly, suspended platelets were mixed with 1 mM calcium (Sigma, cat# GF353280607) and 5% autologous platelet-poor plasma (as a source of fibrinogen) [29], followed by the addition of thrombin, ADP, or collagen. For each measurement, unaggregated platelets (0% light transmission) and blank buffer (100% light transmission) served as references [29]. Platelet aggregation was expressed as the maximal percent change in light transmittance over 6 min after stimulation with the agonists.

2.7. Flow cytometry for detecting platelet activation

The platelet surface expression of P-selectin was detected by flow cytometry to reflect the extent of platelet activation [20]. Briefly, suspended platelets (1×10^6) were incubated with APC-labeled anti-CD41a (Invitrogen, cat# 17-0419-42) and PE-labeled anti-CD62P (Invitrogen, cat# 12-0626-80) for 30 min, fixed with 1% paraformaldehyde HEPES saline, and centrifuged at 800 g for 5 min. The platelet pellets were resuspended in stain buffer, and analyzed on a FACSCalibur flow cytometer (BD Bioscience, Franklin Lakes, USA). Platelets were identified by their characteristic light scattering and specific binding of anti-CD41a. Isotype-matched antibodies were used to control non-specific fluorescence. Data are expressed as the percentage of 10, 000 CD41a + platelets expressing CD62P.

2.8. Detection of the rate of mitochondrial reactive oxygen species (mtROS) production

For quantification of mtROS, platelets were stained with 5 μM of the non-fluorescent probe dihydrorhodamine 123 (Sigma, cat# D1054), which can freely penetrate through the cell membrane, localize in mitochondria, and irreversibly react with mtROS to form fluorescent rhodamine 123 [30]. The fluorescence intensity of rhodamine 123 (λex/em: 490/530 nm) was continuously monitored on a PheraStar FS plate reader (BMG LABTECH, Ortenberg, Germany) every 4 min for 20 min [30]. The acquired raw data were fitted by linear regression to calculate the regression slope, which represented the rate of mtROS generation over time [31].

2.9. Biochemical assays for determining mitochondrial complex activity, the NAD^+/NADH ratio, and ATP contents

The activities of mitochondrial complexes I–V were measured in suspended platelets using spectrophotometric methods as summarized by Rodenburg [32].

The concentrations of NAD^+ and NADH in platelets were measured with the EnzyFluo NAD/NADH assay (BioAssay Systems, cat# EFND-100), which utilizes a non-fluorescent probe to specifically react with NADH to form a fluorescent product. The fluorescence intensity of this product at λex/em = 530/585 nm was read by a PheraStar FS plate reader to quantify NAD^+, NADH, and their ratio following the manufacturer's instructions.

The ATP concentrations of platelets were determined using the EnzyLight ATP assay (BioAssay Systems, cat# EATP-100). Briefly, platelets were lysed by a single working reagent to release ATP, which reacted with the ATP-dependent luciferin-luciferase system. The light intensity, as a direct measure of the ATP contents, was detected on a PheraStar FS plate reader within 1 min after adding the assay reagent.

2.10. Statistical analysis

For the bioenergetic data, individual group samples were compared using the unpaired *t*-test; ex vivo comparisons between the treatment

group and the vehicle group were made by the paired *t*-test; multiple comparisons were performed using one-way ANOVA with the LSD post hoc test.

For the metabolomic data, a supervised model of orthogonal partial least-squares discriminate analysis (OPLS-DA) was conducted to compare the global differences between groups, and to assess the importance of each metabolite in OPLS-DA by calculating the Variable Influence on Projection scores. The goodness of fit and predictability of OPLS-DA were evaluated by a 200-permtation test. Differential comparisons of single metabolites were performed using the Wilcoxon rank-sum test, with the Benjamini–Hochberg procedure to control the false discovery rate (FDR) [33]. Metabolites with FDR <0.05 and fold changes >4/3 or <3/4 were considered differentially abundant [34]. All the above analyses were conducted using R (v 3.5.3).

The integration of bioenergetics and metabolomics was performed using the xMWAS tool [35], in which sparse partial least-squares regression was conducted to calculate the pairwise correlations between bioenergetic and metabolomic features. Then, the multilevel community detection algorithm was executed to identify a series of clusters containing metabolic and bioenergetic nodes that were highly connected with each other (|r| > 0.4, P < 0.05). We used MetaboAnalyst 5.0 [36] to conduct metabolic pathway analysis for each bioenergetic feature independently. Significant pathways had to match at least 4 metabolites and have a *P* value of <0.05 [37].

3. Results

3.1. Bioenergetics in resting platelets

For standardized testing, platelets of all study participants were freshly isolated, and seeded in XF DMEM at a density of 1×10^7 per well [15,22]. Both OCRs and ECARs of platelets were stable for at least 3 h (Supplementary Fig. 2A). Detecting the surface expression of CD62P did not reveal platelet activation induced by seeding or bioenergetic measurement (Supplementary Fig. 2B).

Then, we sought to measure the mitochondrial respiration profiles in resting platelets (Fig. 1 A and Supplementary Table 1). The basal respiration was first measured, then oligomycin (complex V inhibitor) was added to quantify OCRs linked to proton leak and ATP synthesis [7]. Diabetic patients with LST exhibited no significant alterations in basal respiration, proton leak, or ATP-linked respiration compared with diabetic patients without LST (non-LST, Fig. 1B) or healthy subjects (Supplementary Table 1). Further addition of FCCP for uncoupling electron flux resulted in a slightly lower rate (by 12%, Fig. 1B) of maximal respiration in LST platelets than in non-LST platelets. Final injection of rotenone (CI inhibitor) and antimycin A (complex III inhibitor) completely blocked the mitochondrial electron transport chain to allow monitoring of the non-mitochondrial OCR [7], which was not significantly altered in LST platelets. Additionally, we did not find significant differences in glycolytic profiles between the LST, non-LST, and healthy control groups (Fig. 1C and D and Supplementary Table 1).
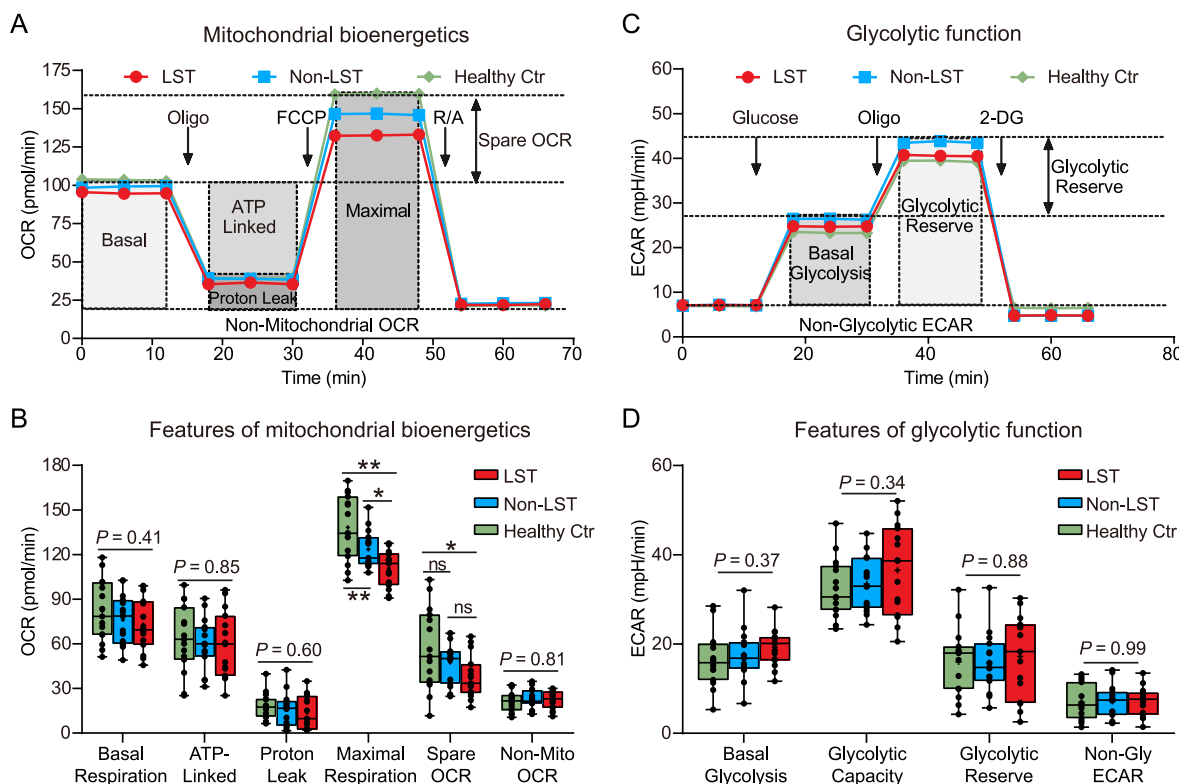
Fig. 1. Profiles of mitochondrial respiration and glycolytic function are largely unchanged in resting platelets from type 2 diabetic patients who developed LST. (**A**) Definition of platelet mitochondrial respiration. (**B**) Comparisons of mitochondrial respiratory parameters in resting platelets from diabetic patients with LST (red, n = 15), diabetic patients without LST (blue, n = 15), and healthy controls (green, n = 15). *P < 0.05; **P < 0.001; ns, nonsignificant. (**C**) Definition of platelet glycolytic function. (**D**) Comparisons of glycolytic parameters in resting platelets from diabetic patients with LST (red, n = 15), diabetic patients without LST (blue, n = 15), and healthy controls (green, n = 15). Data are mean ± SD. Oligo indicates oligomycin; R/A, rotenone/antimycin A; 2-DG, 2-deoxy-glucose; OCR, oxygen consumption rate; ECAR, extracellular acidification rate. (For interpretation of the references to colour in this figure legend, the reader is referred to the Web version of this article.)

3.2. Bioenergetics in activated platelets

To further describe the bioenergetic characterization of platelets in the activated state, the Mitochondrial Stress test was also performed in thrombin-activated (0.1 U/mL) platelets. As presented in Fig. 2A and B, adding thrombin induced a subtle increase (by 28%) in basal OCR in non-LST platelets, while the thrombin-induced increase (by 5%, $P = 0.007$) in basal OCR was almost eliminated in LST platelets. Furthermore, we found a much stronger effect of oligomycin on inhibiting OCR and a much weaker effect of FCCP on releasing maximal OCR (Fig. 2A), compatible with the substantial decreases in ATP-linked ($P = 0.008$, Fig. 2C) and maximal respiration ($P = 1.8E-11$, Fig. 2D), in platelets from LST patients. Consistent with a recent report by Avila et al. [38], we observed a slight but significant reduction in both basal and maximal respiration in diabetic patients without LST compared with those of healthy subjects (Supplementary Table 2), which suggested a certain degree of bioenergetic impairment in diabetic platelets. In the comparison of diabetic patients with LST with healthy subjects, the changes in platelet bioenergetics became more substantial, but the change patterns were generally similar to those in the comparison of LST with non-LST patients (Supplementary Table 2).

Considering that aerobic glycolysis may compensate for impaired mitochondrial respiration to sustain the energy need during platelet activation [39], we continued to monitor the glycolytic profiles of activated platelets. We first observed a strong effect of thrombin on increasing the basal ECAR (by 94%, Fig. 2E), which suggested an increased energy demand during platelet activation. Then, following the addition of glucose and oligomycin, activated platelets from LST patients displayed significant increases in both basal glycolysis and maximal glycolytic capacity compared with non-LST (Fig. 2F and G) or healthy platelets (Supplementary Table 2). This was potentially the reason for the unchanged ATP contents in activated platelets from LST patients compared with those in non-LST platelets (Fig. 2H).

To investigate whether the aberrant mitochondrial respiration in LST platelets was linked with a specific enzymatic deficiency, we measured the enzymatic activity of each mitochondrial complex (I–V). Although the activities of complexes II-V were similar between LST and non-LST platelets, we did observe a significant reduction (by 33%, $P = 1.3E-7$, Fig. 2I) in CI activity in LST patients. Congruently, the CI-dependent OCR was also decreased by 30% ($P = 1.1E-7$, Fig. 2J and K) in LST platelets when respiring on CI-selective substrates. As CI is the major site controlling NADH oxidation [40], we reasoned that the reduced CI activity might alter the $NAD^+/NADH$ redox state. Indeed, platelets from LST patients exhibited a substantial reduction in NAD^+ levels, a subtle increase in NADH levels, and a more than 60% decrease in the $NAD^+/NADH$ ratio ($P = 1.8E-6$, Fig. 2L), accompanied by a higher production rate of mtROS (Fig. 2M).

In parallel with these bioenergetic aberrancies, thrombin seemed to induce greater platelet aggregation in LST platelets than in non-LST platelets, especially at low to intermediate doses (Fig. 2N and Supplementary Fig. 3). A similar tendency for greater aggregation was also observed in LST platelets in response to ADP and collagen (Supplementary Fig. 3). As granule secretion plays essential roles in the amplification of platelet signaling and consequent aggregation [41], we continued to measure α-granule secretion by detecting surface P-selectin expression. Thrombin-induced P-selectin exposure was found to be significantly increased in LST platelets, further validating the hyperreactive status of LST platelets (Fig. 2O).

3.3. Partial inhibition of CI activity mimics the bioenergetic changes in LST platelets

To explore the mechanistic link of CI inhibition with platelet bioenergetic dysfunction, we analyzed the dose-response effects of CI inhibition by using different doses of rotenone to culture platelets from diabetic patients without LST (non-LST). Exposure to high-dose rotenone (500 nM) led to an almost complete loss of CI activity, accompanied by an entirely inverted ratio of $NAD^+/NADH$, a more than 80% decrease in OCRs, and an up to 3-fold increase in mtROS (Supplementary Fig. 4). Such severe damage to mitochondrial bioenergetics has been reported to be more likely to induce platelet apoptosis rather than platelet activation [42], which was highly different from that observed in LST platelets. This might explain the observation of no significant effects of high-dose rotenone treatment on thrombin-, ADP-, or collagen-initiated platelet aggregation (Supplementary Fig. 4E).

In contrast, treatment with rotenone at a low dose of 50 nM caused a 34% reduction in CI activity (Fig. 3A), which was a fall similar to that in LST platelets. This degree of CI inhibition led to 20–60% decreases in ATP-linked OCR (by 40%), maximal OCR (by 24%), and the $NAD^+/NADH$ ratio (by 60%, Fig. 3B–E) as well as significant increases in glycolysis, mtROS, and platelet aggregation (Fig. 3F–J), thus mimicking the bioenergetic changes in LST platelets. Interestingly, the effect of low-dose rotenone exposure might be associated with diabetic status, because in healthy platelets, treatment with low-dose rotenone had a much smaller effect on the bioenergetic profiles and platelet aggregation (Supplementary Fig. 5). Collectively, these data suggest that in the context of T2DM, partial but incomplete inhibition of CI activity can recapitulate the pattern of bioenergetic aberrancies observed in LST platelets.

## 3.4. Metabolomics in activated platelets

To further elucidate the metabolic changes underlying the bioenergetic aberrancy in LST patients, we further performed untargeted metabolomic profiling in platelets preactivated by thrombin. Similar to previous reports [15], we annotated up to 943 metabolites in activated platelets. The OPLS-DA plot depicted a significant difference in global metabolome profiles between diabetic patients with and without LST (Fig. 4A). The goodness of fit and predictability of OPLS-DA were validated by 200-permutation testing, which showed small variances in cross-validated Q^2 and R^2 (Fig. 4B). At the thresholds of FDR <0.05 and fold changes <3/4 or >4/3, a total of 155 metabolites were differentially abundant in LST versus non-LST platelets, with 84 downregulated and 71 upregulated metabolites (Fig. 4C and Supplementary Table 3).

The downregulated metabolites strongly affected pathways of the tricarboxylic acid (TCA) cycle, NAD^+ biosynthesis, and glutamine metabolism (Fig. 4D). Specifically, almost all TCA cycle metabolites were significantly decreased in LST platelets (Fig. 4E). Of note, isocitrate, α-ketoglutarate, and malate, as the key metabolites of the TCA cycle involved in NADH generation, were among the top 5 downregulated metabolites (Supplementary Table 3). The downregulation of the TCA cycle in LST platelets was also accompanied by reduced abundances of several NAD^+ precursors (nicotinic acid, nicotinamide riboside, nicotinamide mononucleotide, and nicotinamide, Fig. 4F), which was in agreement with the observation of an imbalanced $NAD^+/NADH$ ratio in LST platelets. In addition, L-glutamine, as a precursor of α-ketoglutarate that fills the TCA cycle [22], was also downregulated (73%) in LST patients (Fig. 4D).

In contrast, platelets from LST patients showed more than 2-fold increases in the abundances of several proximal glycolytic metabolites (glucose-6-phosphate, fructose-6-phosphate, and fructose-1,6-bisphosphate) compared with non-LST platelets (Fig. 4D). Interestingly, the distal glycolytic metabolites (pyruvate and lactate) related to NAD^+ regeneration did not significantly change in LST platelets (Fig. 4D and G). The imbalance between proximal and distal glycolytic metabolites might induce an increased conversion of glucose into the pentose phosphate pathway (PPP) [22], leading to significant upregulation of several PPP metabolites (6-phosphogluconase, 6-phosphogluconate, and ribulose-5-phosphate) in LST platelets (Fig. 4D and G). Additionally, since a series of proaggregatory prostaglandins (PGG_2, PGH_2, and PGE_2) [43] were significantly upregulated, LST platelets were suggested to be hyperactivated at the metabolic level compared with non-LST platelets
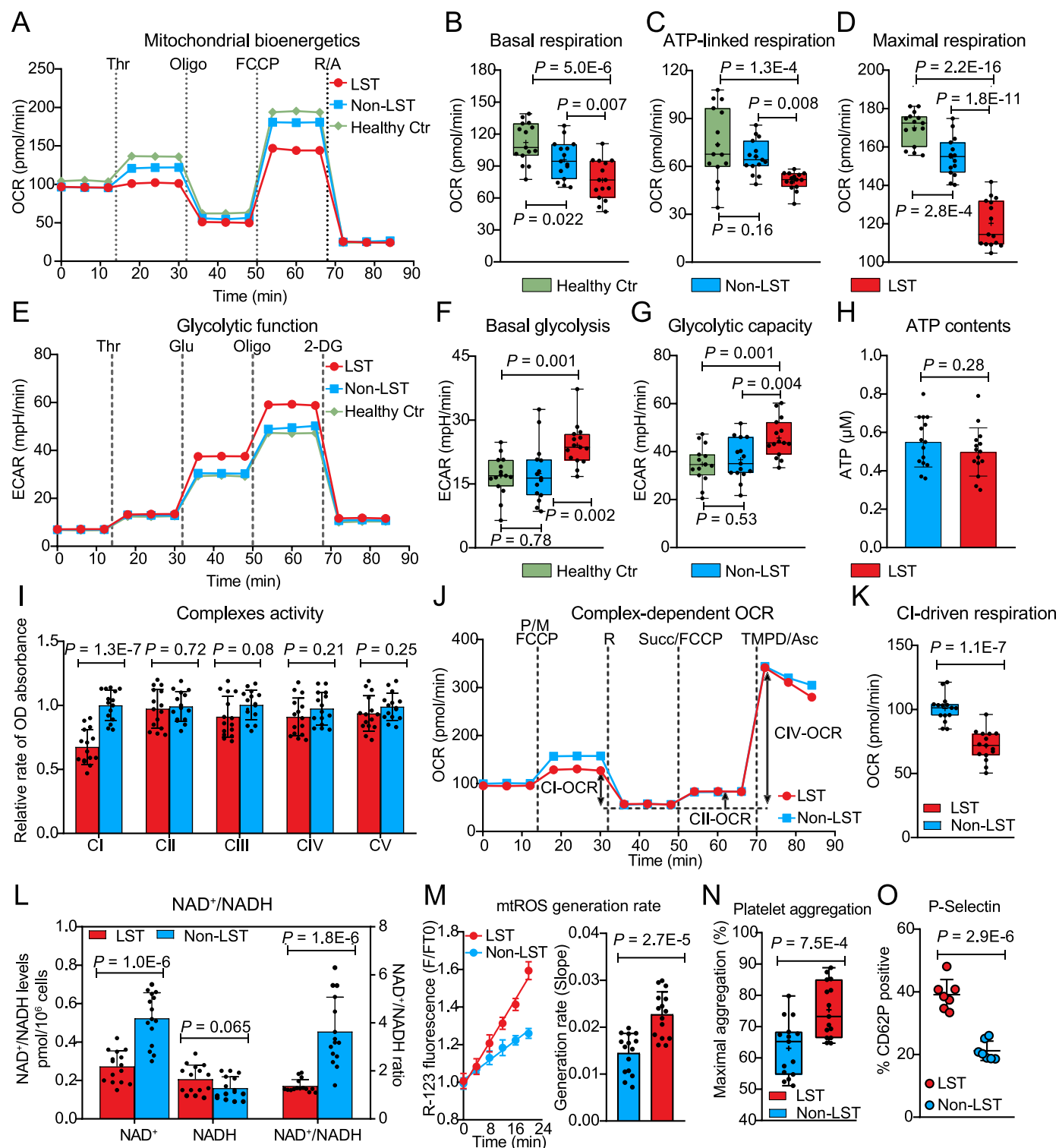
Fig. 2. Aberrant bioenergetic profiles in thrombin-activated platelets from type 2 diabetic patients who developed LST. (**A**) Profiles of mitochondrial respiration in thrombin-activated (0.1 U/mL) platelets. (**B-D**) Basal, ATP-linked, and maximal respiration in LST (n = 15), non-LST (n = 15), and healthy (n = 15) platelets in the activated state. Boxes show the 25–75 percentile; whiskers show the minimum-maximum; lines represent the median; + represents the mean. (**E**) Profiles of glycolytic function in activated platelets. (**F-G**) Basal glycolysis and maximal glycolytic capacity in LST, non-LST, and healthy platelets in the activated state. (**H**) Quantification of ATP contents. (**I**) Enzymatic activities of mitochondrial complexes I–V in LST and non-LST platelets in the activated state. (**J**) Profiles of complex-dependent respiration in activated platelets. (**K**) Quantification of CI-dependent respiration. (**L**) The $NAD^+/NADH$ redox state in LST and non-LST platelets in the activated state. (**M**) Measurement of mtROS production rate. The left picture shows representative mtROS alterations over time from a LST patient and a non LST patient; the right picture shows the comparison of mtROS production rate between LST and non-LST platelets. (**N**) Thrombin-activated aggregation in LST and non-LST platelets. (**O**) Percent of platelets expressing surface P-selectin. Thr indicates thrombin; Oligo, oligomycin; R, rotenone; A, antimycin; 2-DG, 2-deoxy-glucose; OCR, oxygen consumption rate; ECAR, extracellular acidification rate; P, pyruvate; M, malate; Succ, succinate; Asc, ascorbate.
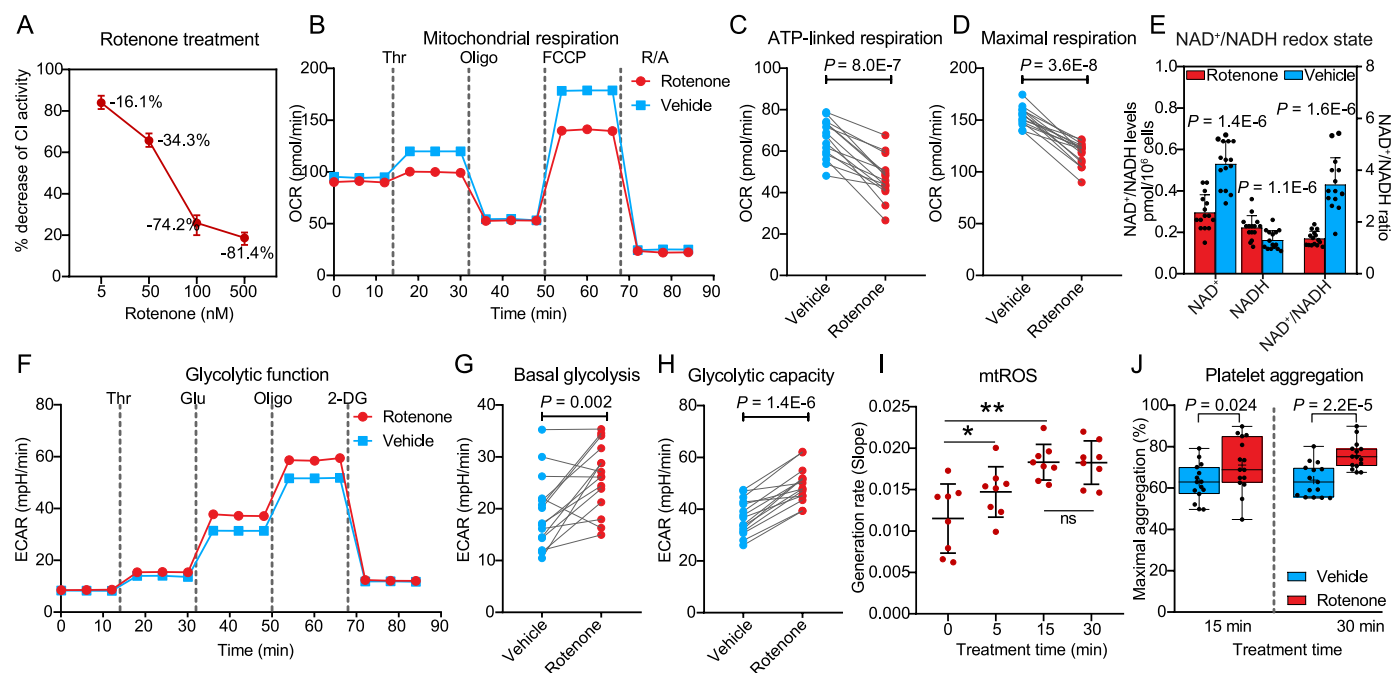
Fig. 3. Complex I inhibition by low-dose rotenone treatment induces bioenergetic dysfunction and platelet aggregation in thrombin-activated platelets from diabetic patients without LST (non-LST). (**A**) Dose effect of rotenone treatment on inhibiting complex I activity. (**B**) Mitochondrial respiration of non-LST platelets after 30-min treatment of vehicle (n = 15) or 50 nM rotenone (n = 15). (**C-D**) ATP-linked and maximal respiration of non-LST platelets after 30-min treatment of vehicle or 50 nM rotenone. (**E**) The NAD$^+$/NADH redox state of non-LST platelets after 30-min treatment of vehicle or 50 nM rotenone. (**F**) Glycolytic function of non-LST platelets after 30-min treatment of vehicle (n = 15) or 50 nM rotenone (n = 15). (**G-H**) Basal glycolysis and maximal glycolytic capacity of non-LST platelets after 30-min treatment of vehicle or 50 nM rotenone. (**I**) Time-dependent effects of rotenone treatment on mtROS production in non-LST platelets (n = 8). *$P < 0.05$; **$P < 0.001$; ns, nonsignificant. (**J**) Thrombin-induced (0.1 U/mL) aggregation of non-LST platelets after 15-min and 30-min treatments of vehicle or rotenone. *P* values determined by paired 2-tailed *t*-test or 1-way ANOVA (for multi-group comparison). Thr indicates thrombin; Oligo, oligomycin; R/A, rotenone/antimycin; 2-DG, 2-deoxy-glucose; OCR, oxygen consumption rate; ECAR, extracellular acidification rate.

(Fig. 4D).

Then, we analyzed the effects of CI inhibition on the global metabolome in non-LST platelets. As shown in Fig. 5A and B, CI inhibition by low-dose rotenone led to a significant change in global metabolomic profiles, including differential changes in the abundances of 134 metabolites (78 downregulated and 56 upregulated metabolites, Supplementary Table 4), in rotenone-treated non-LST platelets. Of note, the rotenone-treated non-LST platelets shared up to 46% (n = 61) of differential metabolites with LST platelets (Fig. 5C). Specifically, rotenone treatment induced widespread downregulation of TCA cycle metabolites and NAD$^+$ precursors as well as upregulation of several proximal glycolytic metabolites (Fig. 5D), generating a metabolomic profile similar to that observed in LST platelets. Collectively, these results concur with the bioenergetic data, suggesting that both the bioenergetic and metabolomic aberrancies observed in LST patients are at least partially caused by deficient CI activity.

3.5. Integration of bioenergetics and metabolomics in activated platelets

We next sought to construct the integrative networks of bioenergetics and metabolomics using xMWAS. In diabetic patients without LST (non-LST), we identified a total of 313 highly connected nodes (|r| > 0.4, $P < 0.05$) between 175 metabolites and 10 bioenergetic features within 5 clusters (Fig. 6A and Supplementary Table 5). Of them, Clusters 1 and 2 encompassed 80 (46%) metabolites having high connections with 6 features of mitochondrial respiration, whereas Clusters 3–5 included 95 (54%) metabolites highly correlated with 4 glycolytic parameters. In contrast, there were much fewer metabolites (n = 58, 32% vs. 54%) connected with glycolytic function in LST platelets. Instead, strong correlations with mitochondrial respiration were identified in up to 125 metabolites within 4 clusters (68% vs. 46%, $P = 1.6E-5$, Fig. 6B

and Supplementary Table 6). Congruently, when calculating the centrality measure to assess the importance of connected nodes, all 6 features of mitochondrial respiration had higher centrality values in LST platelets than in non-LST platelets (Supplementary Table 7), demonstrating a more important role of mitochondrial respiration in integrative networks of LST patients. Interestingly, when the non-LST platelets were pretreated with low-dose rotenone, the proportion of metabolites connected with mitochondrial respiration significantly increased to 72% (vs. 46%, $P = 5.5E-8$, Supplementary Fig. 6 and Supplementary Table 8), which was statistically more similar to that in LST platelets (68%, $P = 0.38$).

Then, we performed pathway enrichment analyses for metabolites within each cluster. In non-LST platelets (Fig. 6C), both mitochondrial respiration and glycolytic features were connected with a series of metabolic pathways, generally involving metabolism of carbohydrates (TCA cycle, PPP, glycolysis, etc.), vitamins (nicotinamide, folate), amino acids (alanine, aspartate, glutamate, etc.), and lipids (arachidonic acids, glycerophospholipids). In LST platelets (Fig. 6D), the impacts of mitochondrial respiration on metabolic pathways were still strong and broad, while pathways associated with glycolytic features were mainly limited to glycolysis-related pathways (i.e. glycolysis, gluconeogenesis, and PPP). Taken together, the integrative network analysis suggests that the metabolomic alterations in LST patients may be attributed primarily to mitochondrial respiratory impairment rather than increased glycolysis.

3.6. Protection against CI inhibition: role of mtROS scavenging and NAD$^+$/NADH rebalance

Understanding how CI inhibition induces bioenergetic aberrancies may provide insight into the causal link between CI inhibition and
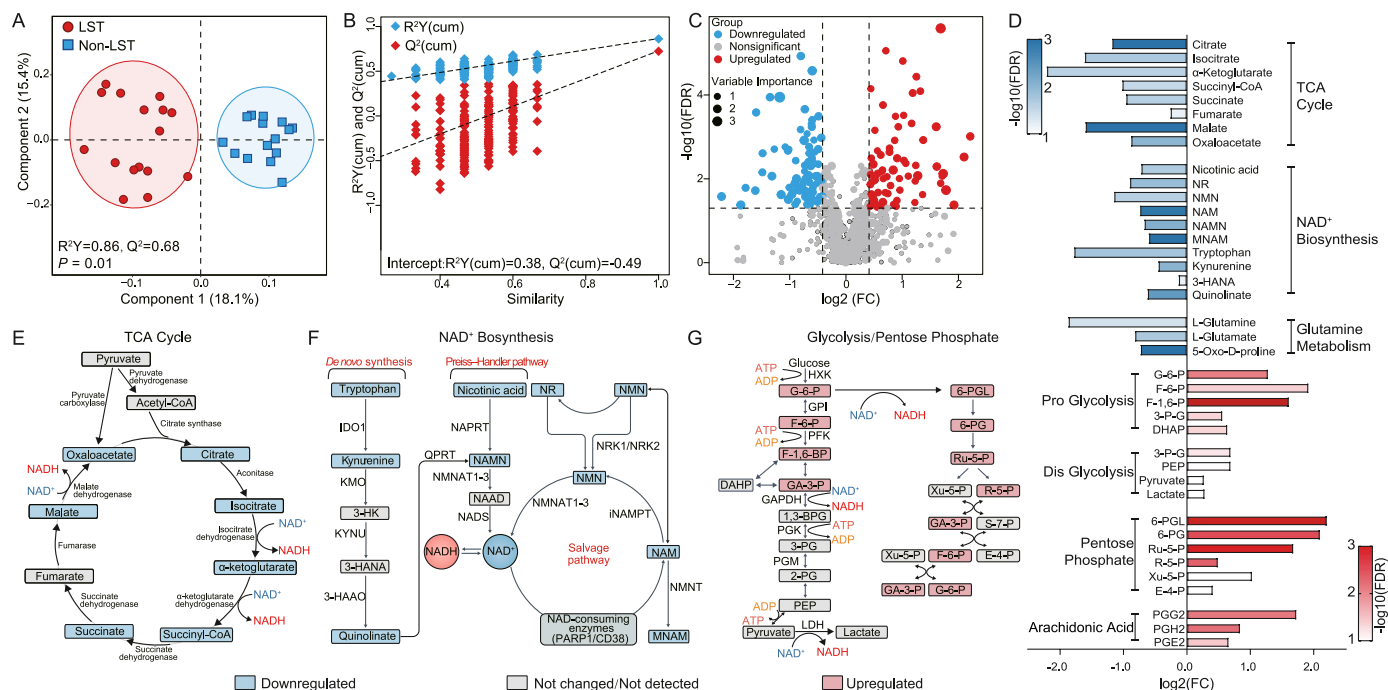
Fig. 4. Aberrant metabolomic profiles in thrombin-activated platelets from type 2 diabetic patients who developed LST. (**A**) The OPLS-DA plot shows the global metabolomic difference between LST (n = 15) and non-LST (n = 15) platelets at the activated state. (**B**) The 200-permutation test confirms the goodness of fit and predictability of OPLS-DA. (**C**) The volcano plot shows the differential abundant pattern of 943 metabolites between LST and non-LST platelets at the activated state. (**D**) Effect sizes of metabolites in pathways of tricarboxylic acid (TCA) cycle, NAD$^+$ biosynthesis, glutamine, glycolysis, pentose phosphate, and arachidonic acid metabolism. (**E**) TCA cycle. (**F**) NAD$^+$ biosynthetic pathway. (**G**) Glycolytic and pentose phosphate pathways. Blue rectangles indicate metabolites downregulated in LST platelets; red, metabolites upregulated in LST platelets; grey, no change or not detected. NR indicates nicotinamide riboside; NMN, nicotinamide mononucleotide; NAM, nicotinamide; NAMN, nicotinic acid mononucleotide; MNAM, methylnicotinamide; 3-HANA, 3-hydroxyanthranilic acid, G-6-P, glucose-6-phosphate; F-6-P, fructose-6-phosphate; F-1,6-BP, fructose-1,6-bisphosphate; GA-3-P, glyceraldehyde-3-phosphate; DHAP, dihydroxyacetone phosphate; 3-PG; 3-phosphoglycerate; PEP, phosphoenolpyruvate; 6-PGL, 6-phosphonoglucono-lactone; 6-PG, 6-phosphogluconate; Ru-5-P, ribulose-5-phosphate; R-5-P, ribose-5-phosphate; Xu-5-P, xylulose-5-phosphate; E−4-P, erythrose-4-phosphate. (For interpretation of the references to colour in this figure legend, the reader is referred to the Web version of this article.)

platelet abnormalities in LST patients. One potential explanation is that CI inhibition causes increased production of mtROS, which may impair mitochondrial respiration and boost platelet aggregation [7,44]. However, treating LST platelets with MitoQ, a mitochondria-targeted ROS scavenger, failed to improve ATP-linked or maximal respiration but markedly blunted platelet aggregation (Supplementary Fig. 7). These results validate the role of mtROS as a second messenger inducing platelet activation [7], but cannot establish the direct link between mtROS and impaired mitochondrial respiration.

Having observed that inhibiting CI could substantially decrease NAD$^+$ levels and disrupt the NAD$^+$/NADH balance, we next questioned whether normalization of the NAD$^+$/NADH ratio might reverse impaired mitochondrial respiration in LST platelets. To test this hypothesis, LST platelets were supplemented with NR, a NAD$^+$ precursor that maintains NAD$^+$ synthesis in platelets [45]. Indeed, exposure to 1 mM NR for 30 min was able to increase the NAD$^+$/NADH ratio to a level similar to that in non-LST platelets (Fig. 7A). Moreover, NR supplementation effectively improved mitochondrial respiration while suppressing mtROS generation and platelet aggregation (Fig. 7C–G).

Another orthogonal method to increase NAD$^+$ bioavailability may be the inhibition of NAD$^+$ consumption [46]. Thus, we incubated LST platelets with olaparib, a clinically approved inhibitor of the major NAD$^+$ consuming enzyme PARP1 [47]. The inhibition of PARP1 by 20 μM olaparib successfully increased the NAD$^+$/NADH ratio (Fig. 7B), accompanied by significant upregulation of mitochondrial respiration and partial inhibition of mtROS production and platelet aggregation in LST platelets (Fig. 7C–G). Importantly, a similar effect of NR or olaparib treatment on normalizing mitochondrial respiration, mtROS production, and platelet aggregation was also found in non-LST platelets pretreated

with low-dose rotenone (Fig. 7H–J). Collectively, our data suggest that rebalancing the NAD$^+$/NADH redox state may protect diabetic platelets against the proaggregatory effects of CI inhibition.

To further examine the relationship between NAD$^+$ metabolism, mtROS production, and platelet aggregation, we incubated the rotenone-treated non-LST platelets with MitoParaquat, a mitochondrial ROS generator that selectively induces redox cycling at CI [48]. As shown in Fig. 7H–J, addition of MitoParaquat (0.1 μM) abolished the inhibition of platelet aggregation by NR or olaparib, (Fig. 7H), but did not interrupt the NR- or olaparib-induced improvements in mitochondrial respiration (Fig. 7J). Together, our data support the idea that partial inhibition of CI may cause impaired homeostasis of NAD$^+$ metabolism first, which further induces the leakage of mtROS at CI and consequently boosts platelet aggregation.

4. Discussion

Platelets are a sort of cells having high metabolic flexibility, which means that platelets can switch freely between multiple bioenergetic pathways to maintain basal energy supply under normal conditions [39]. However, under diabetic conditions that may have induced systematic alterations in bioenergetics and metabolism [49], further inhibition of a certain bioenergetic pathway may impact platelet function more significantly, thus causing platelet abnormalities and thrombotic complications [42,50]. To better delineate the bioenergetic changes during the progression from T2DM to thrombotic complications, our study, for the first time, characterized the bioenergetic profiles of both resting and activated platelets from type 2 diabetic patients who suffered from LST. First, we found that resting platelets from LST patients
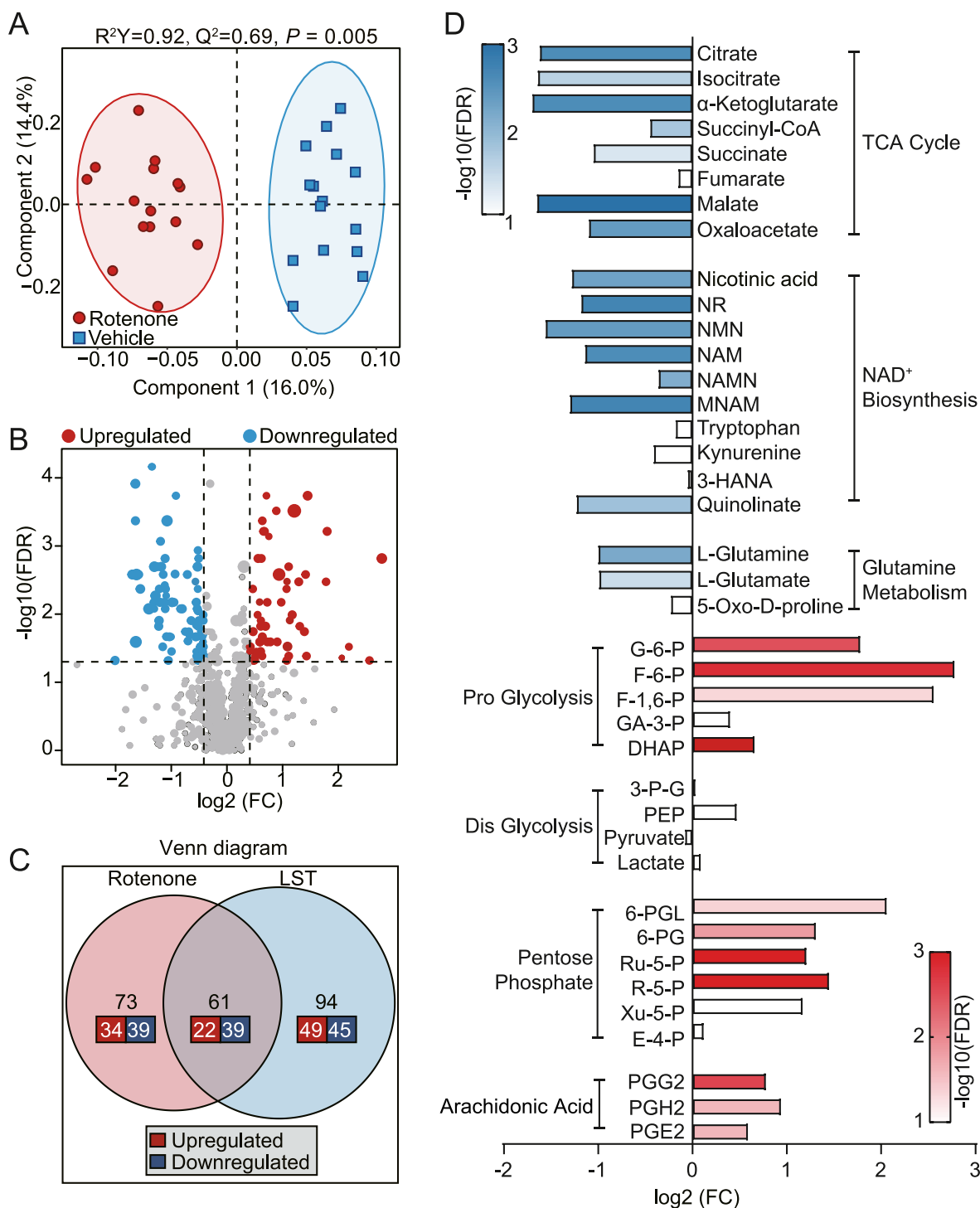
Fig. 5. Metabolomic aberrancies induced by complex I inhibition via low-dose rotenone treatment in thrombin-activated platelets from diabetic patients without LST (non-LST). (**A**) The OPLS-DA plot shows the global metabolomic difference between vehicle- (n = 15) and rotenone-treated non-LST (n = 15) platelets at the activated state. (**B**) The volcano plot shows the differential abundant pattern of metabolome between vehicle- and rotenone-treated non-LST platelets at the activated state. (**C**) The Venn diagram identifies common differential metabolites between LST and rotenone-treated non-LST platelets. (**D**) Effect sizes of metabolites in pathways of tricarboxylic acid (TCA) cycle, NAD$^+$ biosynthesis, glutamine, glycolysis, pentose phosphate, and arachidonic acid metabolism. NR indicates nicotinamide riboside; NMN, nicotinamide mononucleotide; NAM, nicotinamide; NAMN, nicotinic acid mononucleotide; MNAM, methylnicotinamide; 3-HANA, 3-hydroxyanthranilic acid, G-6-P, glucose-6-phosphate; F-6-P, fructose-6-phosphate; F-1,6-BP, fructose-1,6-bisphosphate; GA-3-P, glyceraldehyde-3-phosphate; DHAP, dihydroxyacetone phosphate; 3-PG; 3-phosphoglycerate; PEP, phosphoenolpyruvate; 6-PGL, 6-phosphonoglucono-lactone; 6-PG, 6-phosphogluconate; Ru-5-P, ribulose-5-phosphate; R-5-P, ribose-5-phosphate; Xu-5-P, xylulose-5-phosphate; E−4-P, erythrose-4-phosphate.
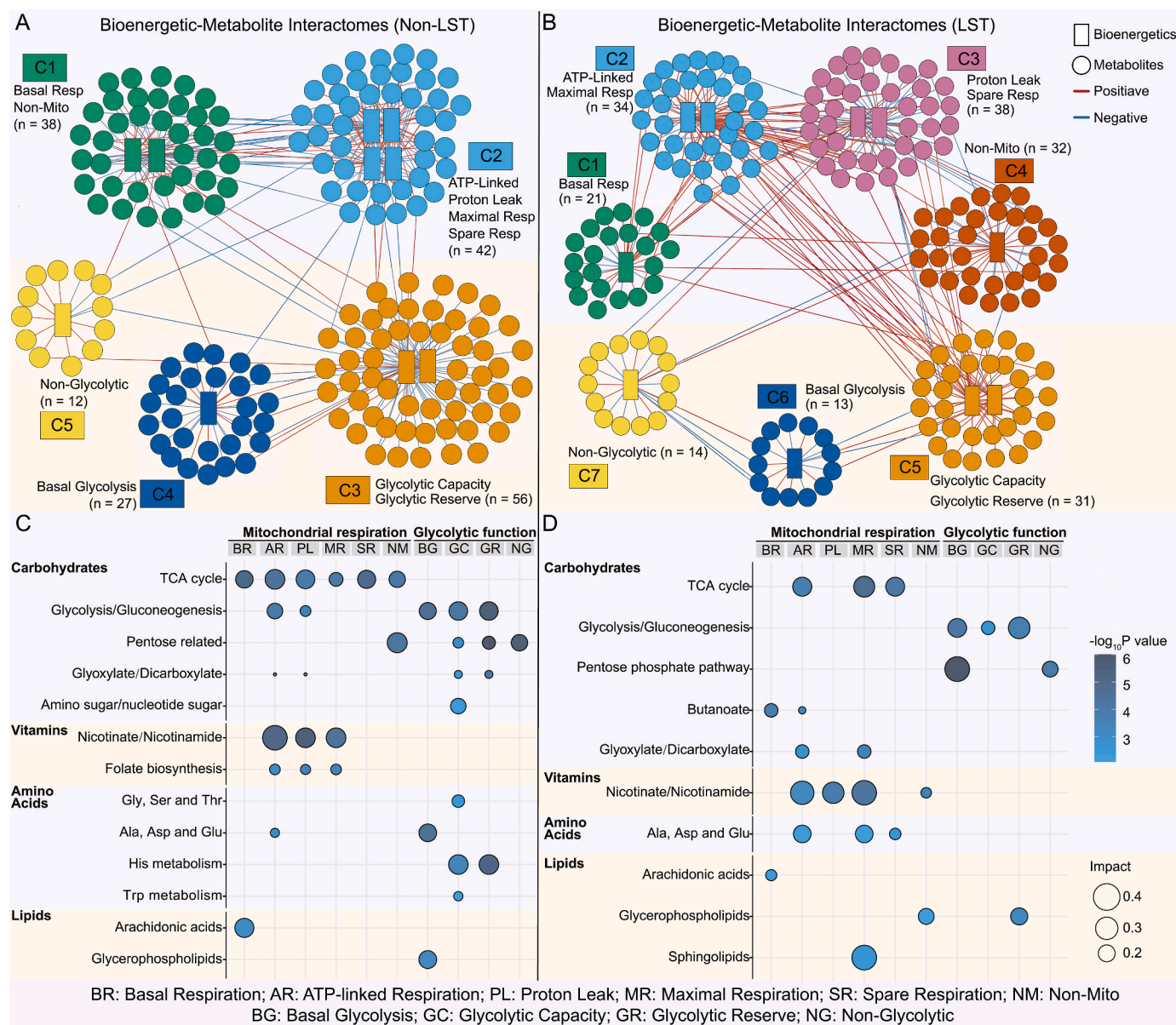
Fig. 6. Bioenergetics-metabolite interactomes in thrombin-activated platelets from diabetic patients with (n = 15) and without (n = 15) LST. (**A-B**) Integrative network of bioenergetic and metabolomic features in non-LST (**A**) and LST (**B**) platelets at the activated state. Metabolites are depicted as circles and bioenergetic features as rectangles. Red lines indicate positive associations; blue lines indicate negative associations. (**C-D**) Metabolic pathways associated with each bioenergetic feature in non-LST (**C**) and LST (**D**) platelets at the activated state. Significant pathways must include at least 4 matched metabolites and have a *P* value of <0.05. Size of the circle maps to the impact of bioenergetic features on metabolic pathways, transparency of the circle maps to the corresponding *P* value. Resp indicates respiration; TCA, tricarboxylic acid; Ala, alanine; Asp, aspartate; Glu, glutamate; Gly, glycine; Ser, serine; Thr, threonine; His, histidine; Trp, tryptophan. (For interpretation of the references to colour in this figure legend, the reader is referred to the Web version of this article.)

exhibited a lower rate of maximal respiration than non-LST platelets, but with no alterations in other parameters of mitochondrial respiration including ATP-linked OCR, spare OCR, and proton leak. Physiologically, quiescent platelets only work at a small fraction of their maximal OXPHOS, and reserve a large respiratory capacity to ensure energy supply under stress conditions [51]. So although the maximal OXPHOS has already declined in LST platelets, their spare respiratory capacity might still be sufficient to maintain mitochondrial ATP production and proton gradient. However, in the presence of activating stimuli that increased energetic demands substantially, the mitochondrial bioenergetics of LST platelets was severely compromised, as evidenced by the insufficient spare respiratory capacity to respond to thrombin stimulation as well as the full-scale downregulation of basal, maximal, and ATP-linked respiration.

Interestingly, although LST platelets had impaired mitochondrial respiration in the activated state, their total ATP contents were not decreased. The maintenance of ATP production in LST platelets might be attributed to the significant upregulation of glycolytic profiles. This metabolic shift to glycolysis, in the presence of impaired mitochondrial respiration, may represent a conserved immunometabolic pattern that essentially reflects the nature of the high metabolic flexibility of platelets [39,52]. Indeed, despite being a less efficient energy-producing pathway, glycolysis may better support a rapid need for ATP production in response to enhanced platelet aggregation in LST platelets [39].

Importantly, the imbalance of mitochondrial respiration and glycolytic function in LST platelets could be reflected at the metabolic level. To be specific, the untargeted metabolomics revealed a dramatic change in global metabolic profiles in LST platelets, with proximal glycolytic
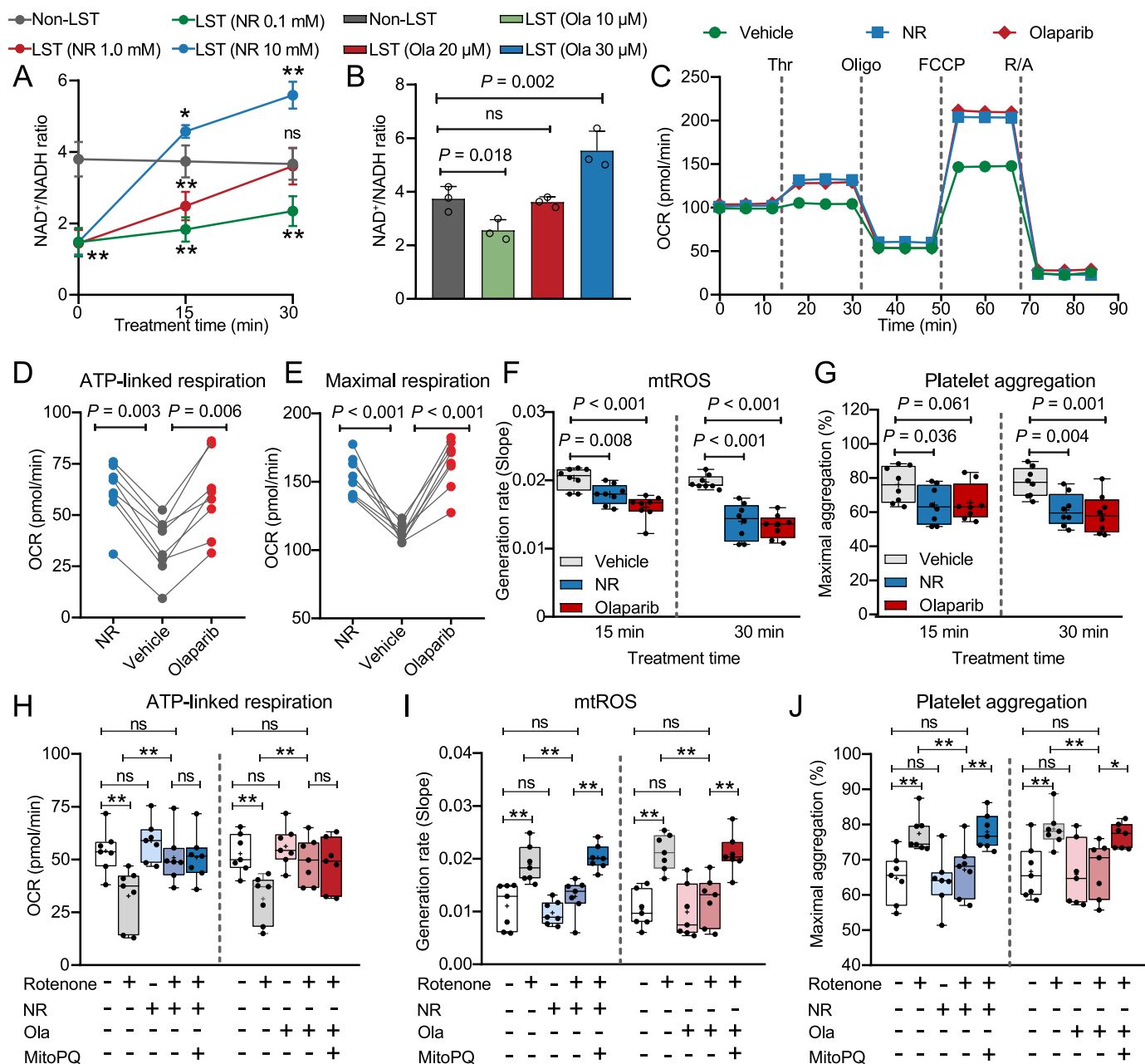
Fig. 7. Rebalancing the NAD$^+$/NADH redox state by NR or olaparib attenuates bioenergetic dysfunction and platelet aggregation. (**A**) Dose- and time-dependent effects of NR treatment on NAD$^+$/NADH ratios. (**B**) Dose-dependent effect of olaparib treatment on NAD$^+$/NADH ratios. (**C-E**) Effects of NR (1.0 mM) or olaparib (20 μM) treatment on mitochondrial respiratory profiles (**C**), ATP-linked respiration (**D**), and maximal respiration (**E**) in LST platelets (n = 8 for each group). (**F**) Effects of NR (1.0 mM) or olaparib (20 μM) treatment on mtROS production in LST platelets. (**G**) Effects of NR (1.0 mM) or olaparib (20 μM) treatment on platelet aggregation in LST platelets. (**H-J**) Effects of NR (1.0 mM) or olaparib (20 μM) treatment on ATP-linked respiration (**H**), mtROS production (**I**), and platelet aggregation (**J**) in rotenone-treated non-LST platelets (n = 7 for each group). *$P < 0.05$; **$P < 0.001$; ns nonsignificant. NR indicates nicotinamide riboside; Ola, olaparib; Thr, thrombin; Oligo, oligomycin; R/A, rotenone/antimycin; MitoPQ, MitoParaquat.

metabolites being raised and mitochondrial TCA cycle being substantially impaired. Considering that studying each metabolic pathway may not fully reflect the complexity of platelet metabolism [53], we further integrated metabolomics with bioenergetic data using a multi-omic approach, which may elucidate the differential networks of metabolic pathways in response to the given bioenergetic changes [14]. In the instance of LST platelets, a large number of metabolic pathways, involving a series of carbohydrates, vitamins, amino acids, and lipids, were found to be connected with the profiles of mitochondrial respiration, but few of them were correlated with glycolytic parameters. The non-LST platelets, by contrast, exhibited a distinct network composition that linked mitochondrial respiration and glycolytic profiles together

through a number of shared metabolic pathways. These results are meaningful, because they promote the understanding of how the platelet metabolome interacts with bioenergetics, highlighting that in the context of LST, the metabolomic alterations of platelets are probably driven by impairment of mitochondrial respiration, but not by compensatory increase in glycolysis.

The observation of the substantial declines in both CI activity and CI-dependent respiration in LST platelets may provide an enzymatic basis for the observed bioenergetic aberrancies. Furthermore, partial inhibition of CI in non-LST platelets by low-dose rotenone successfully recapitulated the bioenergetic aberrancies observed in LST platelets and significantly enhanced platelet aggregation, suggesting a possible

mechanistic link between CI inhibition, bioenergetic aberrancies, and platelet hyperaggregability. CI, as the gatekeeper of the electron transport chain, catalyzes the oxidation of NADH, which provides up to 40% of the proton-motive force utilized for mitochondrial ATP production [54]. If the process of NADH oxidation is inefficient, protons may escape from CI and react with ambient oxygen to produce mtROS [40], which is closely related to platelet hyperactivation possibly through modulation of arachidonic acid metabolism [7]. Our study further supported the linkage between mtROS and platelet aggregation by showing that both mtROS and proaggregatory metabolites of arachidonic acids were upregulated in LST platelets and that scavenging mtROS could blunt rotenone-induced platelet aggregation.

Another direct consequence of CI inhibition may be the dysregulation of NADH oxidation, which damages NAD^+ turnover and causes an imbalanced $NAD^+/NADH$ redox state [55]. Generally, NAD^+ turnover is maintained by common controls of NAD^+-regenerating (CI, LDH, and malate-aspartate shuttle), NAD^+ biosynthetic (salvage or de novo synthesis), and NAD^+-consuming pathways (PARP1 and CD38) [56]. We decided not to modulate NAD^+ regeneration to balance the $NAD^+/NADH$ ratio, because targeting LDH or the malate-aspartate shuttle may exert additional impacts on glycolysis and OXPHOS [57]. Considering that platelets contain an enzymatic system to metabolize NR into NAD^+ [45], we directed our attention toward NR, a NAD^+ precursor that has cardioprotective effects in animal models of heart failure and cardiomyopathy [58,59]. We found that supplementation with NR could preserve mitochondrial respiration, in conjunction with the inhibition of mtROS production and platelet aggregation, in both LST and rotenone-treated non-LST platelets. Congruently, we observed a similar effect of reducing NAD^+ consumption by the PARP1 inhibitor (olaparib) against CI inhibition. These findings provide ex vivo evidence that pharmacologically targeting NAD^+ metabolism may be effective against platelet hyperaggregability induced by CI defects.

It is well known that diabetes may accelerate the production of ROS and damage mitochondrial function, possibly through transduction of the aldose reductase pathway [42,50]. Excessive ROS can then stimulate platelet aggregation through activation of the PLCγ2/PKC/p38α MAPK pathway, a hyperactive Ca^{2+} response to stimulation, and further induction of thromboxane [7,50], while the severity of mitochondrial dysfunction may determine whether diabetic platelets are prone to be apoptotic (severe) or hyperactive (modest) [42]. Here, our study deepens the understanding of the relationship between impaired NAD^+ metabolism, mtROS overproduction, and platelet aggregation in an ex vivo model of mitochondrial dysfunction — diabetic platelets with partial inhibition of CI. We found that pharmacological induction of CI-sourced mtROS abolished the NR- or olaparib-induced inhibition of platelet aggregation, while downregulating mtROS by MitoQ did not improve mitochondrial respiration. Taking all the ex vivo data together, we suggest that the $NAD^+/NADH$ imbalance resulting from CI inhibition may be the direct cause of mitochondrial respiratory dysfunction, whereas mtROS is more likely downstream of impaired mitochondrial bioenergetics, mediating the effects of dysregulated NAD^+ metabolism on platelet aggregation.

Our study is the first to report the mechanistic link between platelet mitochondrial respiration and LST, with comprehensive delineation of both bioenergetic and metabolomic characterizations in platelets from LST patients. Nevertheless, our study has limitations. First, although the LST and non-LST groups were carefully balanced with respect to a series of clinical, procedural, and pharmacological variables relevant to LST incidence, the case-control design still has the limitations inherent to retrospective inclusion of participants into the 2 groups. We adopted the case-control design mainly because of the rarity of ST occurrence and the large number of platelet samples that would be needed. Second, we elected to collect platelet samples at the end of follow-up, in order to monitor platelet bioenergetics in the stable quiescent phase, but not in the acute phase of the ST episode when many temporary changes of platelet bioenergetics occur [60]. This study design also allowed for a longer follow-up to preclude ST development in the non-LST group. However, it is, therefore, not possible to investigate the role of mitochondrial bioenergetics just prior to the ST episode in the thrombotic process of platelets. Third, antiplatelet treatment, as the standard of care after PCI, was applied in every included patient. Although the use of antiplatelet medications was matched between the LST and non-LST groups, the treatment strategy was still heterogeneous, ranging from dual antiplatelet therapy to aspirin alone and clopidogrel alone. Fourth, due to the reduced availability of platelet samples, some ex vivo experiments were performed only in 7–8 samples in each group. Finally, out study was nested within a prospective cohort of type 2 diabetic patients. This may limit the generalizability of our findings to nondiabetic subjects.

5. Conclusions

Collectively, our study reveals that platelets from type 2 diabetic patients who developed LST possess a specific pattern of bioenergetic aberrancies characterized by an imbalanced $NAD^+/NADH$ redox state, reduced mitochondrial respiration, increased glycolysis, and mtROS overproduction. Subsequent ex vivo experiments suggest that this pattern of bioenergetic aberrancies is probably driven by CI inhibition and leads to platelet hyperaggregability. Further integration of bioenergetic data with metabolomics uncovers the metabolic pathways underlying the observed bioenergetic aberrancies in LST patients, which may have significant implications for using the bioenergetics-metabolite interactome to elucidate the pathogenesis of complex conditions such as LST.

Author contributions

XW contributed to design the work and draft the manuscript. XW, NC, and MG contributed to acquisition, analysis, or interpretation of data for the work. NC, XL, and MG contributed to data presentation and statistical analysis. All authors reviewed the manuscript.

Declaration of competing interest

The authors declare no competing interests.

Data availability

Data will be made available on request.

Appendix A. Supplementary data

Supplementary data to this article can be found online at https://doi.org/10.1016/j.redox.2022.102507.

References

[1] T. Gori, A. Polimeni, C. Indolfi, L. Räber, T. Adriaenssens, T. Münzel, Predictors of stent thrombosis and their implications for clinical practice, Nat. Rev. Cardiol. 16 (2019) 243–256.

[2] T. Kimura, T. Morimoto, Y. Nakagawa, K. Kawai, S. Miyazaki, T. Muramatsu, et al., Very late stent thrombosis and late target lesion revascularization after sirolimus-eluting stent implantation: five-year outcome of the j-Cypher Registry, Circulation 125 (2012) 584–591.

[3] J.W. van Werkum, A.A. Heestermans, A.C. Zomer, J.C. Kelder, M.J. Suttorp, B. J. Rensing, et al., Predictors of coronary stent thrombosis: the Dutch stent thrombosis registry, J. Am. Coll. Cardiol. 53 (2009) 1399–1409.

[4] J. Yuan, G.M. Xu, Early and late stent thrombosis in patients with versus without diabetes mellitus following percutaneous coronary intervention with drug-eluting

stents: a systematic review and meta-analysis, Am. J. Cardiovasc. Drugs 18 (2018) 483–492.

[5] A.I. Vinik, T. Erbas, T.S. Park, R. Nolan, G.L. Pittenger, Platelet dysfunction in type 2 diabetes, Diabetes Care 24 (2001) 1476–1485.

[6] N. Vazzana, P. Ranalli, C. Cuccurullo, G. Daví, Diabetes mellitus and thrombosis, Thromb. Res. 129 (2012) 371–377.

[7] E. Masselli, G. Pozzi, M. Vaccarezza, P. Mirandola, D. Galli, M. Vitale, et al., ROS in platelet biology: functional aspects and methodological insights, Int. J. Mol. Sci. 21 (2020) 4866.

[8] S. Ravera, M.G. Signorello, M. Bartolucci, S. Ferrando, L. Manni, F. Caicci, et al., Extramitochondrial energy production in platelets, Biol. Cell. 110 (2018) 97–108.

[9] S. Rovira-Llopis, C. Bañuls, N. Diaz-Morales, A. Hernandez-Mijares, M. Rocha, V. M. Victor, Mitochondrial dynamics in type 2 diabetes: pathophysiological implications, Redox Biol. 11 (2017) 637–645.

[10] C.M.F. Monaco, M.C. Hughes, S.V. Ramos, N.E. Varah, C. Lamberz, F.A. Rahman, et al., Altered mitochondrial bioenergetics and ultrastructure in the skeletal muscle of young adults with type 1 diabetes, Diabetologia 61 (2018) 1411–1423.

[11] P.A. Kramer, S. Ravi, B. Chacko, M.S. Johnson, V.M. Darley-Usmar, A review of the mitochondrial and glycolytic metabolism in human platelets and leukocytes: implications for their use as bioenergetic biomarkers, Redox Biol. 2 (2014) 206–210.

[12] S.H. Lee, J. Du, J. Stitham, S. Atteya, S. Lee, Y. Xiang, et al., Inducing mitophagy in diabetic platelets protects against severe oxidative stress, EMBO Mol. Med. 8 (2016) 779–795.

[13] L. Wang, Q. Wu, Z. Fan, R. Xie, Z. Wang, Y. Lu, Platelet mitochondrial dysfunction and the correlation with human diseases, Biochem. Soc. Trans. 45 (2017) 1213–1223.

[14] M.R. Smith, B.K. Chacko, M.S. Johnson, G.A. Benavides, K. Uppal, Y.M. Go, et al., A precision medicine approach to defining the impact of doxorubicin on the bioenergetic-metabolite interactome in human platelets, Redox Biol. 28 (2020), 101311.

[15] B.K. Chacko, M.R. Smith, M.S. Johnson, G. Benavides, M.L. Culp, J. Pilli, et al., Mitochondria in precision medicine; linking bioenergetics and metabolomics in platelets, Redox Biol. 22 (2019), 101165.

[16] N.H. Cui, J.M. Yang, X. Liu, X.B. Wang, Poly(ADP-Ribose) polymerase activity and coronary artery disease in type 2 diabetes mellitus: an observational and bidirectional mendelian randomization study, Arterioscler. Thromb. Vasc. Biol. 40 (2020) 2516–2526.

[17] X.B. Wang, N.H. Cui, X. Liu, X. Liu, Mitochondrial 8-hydroxy-2'-deoxyguanosine and coronary artery disease in patients with type 2 diabetes mellitus, Cardiovasc. Diabetol. 19 (2020) 22.

[18] X.B. Wang, N.H. Cui, X. Liu, X. Liu, Joint effects of mitochondrial DNA4977 deletion and serum folate deficiency on coronary artery disease in type 2 diabetes mellitus, Clin. Nutr. 39 (2020) 3771–3778.

[19] D.E. Cutlip, S. Windecker, R. Mehran, A. Boam, D.J. Cohen, G.A. van Es, et al., Clinical end points in coronary stent trials: a case for standardized definitions, Circulation 115 (2007) 2344–2351.

[20] E.N. Pennell, K.H. Wagner, S. Mosawy, A.C. Bulmer, Acute bilirubin ditaurate exposure attenuates ex vivo platelet reactive oxygen species production, granule exocytosis and activation, Redox Biol. 26 (2019), 101250.

[21] A. Braganza, C.G. Corey, A.J. Santanasto, G. Distefano, P.M. Coen, N.W. Glynn, et al., Platelet bioenergetics correlate with muscle energetics and are altered in older adults, JCI Insight 5 (2019), e128248.

[22] P. Kaczara, B. Sitek, K. Przyborowski, A. Kurpinska, K. Kus, M. Stojak, et al., Antiplatelet effect of carbon monoxide is mediated by NAD(+) and ATP depletion, Arterioscler. Thromb. Vasc. Biol. 40 (2020) 2376–2390.

[23] M. Forkink, G.R. Manjeri, D.C. Liemburg-Apers, E. Nibbeling, M. Blanchard, A. Wojtala, et al., Mitochondrial hyperpolarization during chronic complex I inhibition is sustained by low activity of complex II, III, IV and V, Biochim. Biophys. Acta 1837 (2014) 1247–1256.

[24] I. Alesutan, F. Moritz, T. Haider, S. Shouxuan, C. Gollmann-Tepeköylü, J. Holfeld, et al., Impact of β-glycerophosphate on the bioenergetic profile of vascular smooth muscle cells, J. Mol. Med. (Berl.) 98 (2020) 985–997.

[25] X.B. Wang, N.H. Cui, X. Liu, A novel 6-metabolite signature for prediction of clinical outcomes in type 2 diabetic patients undergoing percutaneous coronary intervention, Cardiovasc. Diabetol. 21 (2022) 126.

[26] R. Tautenhahn, G.J. Patti, D. Rinehart, G. Siuzdak, XCMS Online: a web-based platform to process untargeted metabolomic data, Anal. Chem. 84 (2012) 5035–5039.

[27] X. Shen, R. Wang, X. Xiong, Y. Yin, Y. Cai, Z. Ma, et al., Metabolic reaction network-based recursive metabolite annotation for untargeted metabolomics, Nat. Commun. 10 (2019) 1516.

[28] A.K. Boysen, K.R. Heal, L.T. Carlson, A.E. Ingalls, Best-matched internal standard normalization in liquid chromatography-mass spectrometry metabolomics applied to environmental samples, Anal. Chem. 90 (2018) 1363–1369.

[29] G.J. Johnson, L.A. Leis, M.D. Krumwiede, J.G. White, The critical role of myosin IIA in platelet internal contraction, J. Thromb. Haemostasis 5 (2007) 1516–1529.

[30] D. Boulghobra, P.E. Grillet, M. Laguerre, M. Tenon, J. Fauconnier, P. Fança-Berthon, et al., Sinapine, but not sinapic acid, counteracts mitochondrial oxidative stress in cardiomyocytes, Redox Biol. 34 (2020), 101554.

[31] J.A. Coral, C.L. Kitchens, J.L. Brumaghim, S.J. Klaine, Correlating quantitative measurements of radical production by photocatalytic TiO(2) with Daphnia magna toxicity, Environ. Toxicol. Chem. 40 (2021) 1322–1334.

[32] R.J. Rodenburg, Biochemical diagnosis of mitochondrial disorders, J. Inherit. Metab. Dis. 34 (2011) 283–292.

[33] Y. Benjamini, Y. Hochberg, Controlling the false discovery rate: a practical and powerful approach to multiple testing, J R Stat Soc Series B Stat Methodol 57 (1995) 289–300.

[34] X. Shen, C. Wang, N. Liang, Z. Liu, X. Li, Z.-J. Zhu, et al., Serum metabolomics identifies dysregulated pathways and potential metabolic biomarkers for hyperuricemia and gout, Arthritis Rheumatol. 73 (2021) 1738–1748.

[35] K. Uppal, C. Ma, Y.M. Go, D.P. Jones, J. Wren, xMWAS: a data-driven integration and differential network analysis tool, Bioinformatics 34 (2018) 701–702.

[36] Z. Pang, J. Chong, G. Zhou, D.A. de Lima Morais, L. Chang, M. Barrette, et al., MetaboAnalyst 5.0: narrowing the gap between raw spectra and functional insights, Nucleic Acids Res. 49 (2021) W388–W396.

[37] T.R. Sanchez, X. Hu, J. Zhao, V. Tran, N. Loiacono, Y.M. Go, et al., An atlas of metallome and metabolome interactions and associations with incident diabetes in the Strong Heart Family Study, Environ. Int. 157 (2021) 106810.

[38] C. Avila, R.J. Huang, M.V. Stevens, A.M. Aponte, D. Tripodi, K.Y. Kim, et al., Platelet mitochondrial dysfunction is evident in type 2 diabetes in association with modifications of mitochondrial anti-oxidant stress proteins, Exp. Clin. Endocrinol. Diabetes 120 (2012) 248–251.

[39] M. Aibibula, K.M. Naseem, R.G. Sturmey, Glucose metabolism and metabolic flexibility in blood platelets, J. Thromb. Haemostasis 16 (2018) 2300–2314.

[40] W.J. Koopman, L.G. Nijtmans, C.E. Dieteren, P. Roestenberg, F. Valsecchi, J. A. Smeitink, et al., Mammalian mitochondrial complex I: biogenesis, regulation, and reactive oxygen species generation, Antioxidants Redox Signal. 12 (2010) 1431–1470.

[41] Z. Li, M.K. Delaney, K.A. O'Brien, X. Du, Signaling during platelet adhesion and activation, Arterioscler. Thromb. Vasc. Biol. 30 (2010) 2341–2349.

[42] W.H. Tang, J. Stitham, Y. Jin, R. Liu, S.H. Lee, J. Du, et al., Aldose reductase-mediated phosphorylation of p53 leads to mitochondrial dysfunction and damage in diabetic platelets, Circulation 129 (2014) 1598–1609.

[43] S. Braune, J.H. Küpper, F. Jung, Effect of prostanoids on human platelet function: an overview, Int. J. Mol. Sci. 21 (2020) 9020.

[44] G. Petrosillo, F. Matera, N. Moro, F.M. Ruggiero, G. Paradies, Mitochondrial complex I dysfunction in rat heart with aging: critical role of reactive oxygen species and cardiolipin, Free Radic. Biol. Med. 46 (2009) 88–94.

[45] W. Delabie, W. Maes, R. Devloo, M.R. Van den Hauwe, K. Vanhoorelbeke, V. Compernolle, et al., The senotherapeutic nicotinamide riboside raises platelet nicotinamide adenine dinucleotide levels but cannot prevent storage lesion, Transfusion 60 (2020) 165–174.

[46] D.X. Zhang, J.P. Zhang, J.Y. Hu, Y.S. Huang, The potential regulatory roles of NAD(+) and its metabolism in autophagy, Metabolism 65 (2016) 454–462.

[47] J.F. Linares, T. Cid-Diaz, A. Duran, M. Osrodek, A. Martinez-Ordoñez, M. Reina-Campos, et al., The lactate-NAD(+) axis activates cancer-associated fibroblasts by downregulating p62, Cell Rep. 39 (2022), 110792.

[48] A.R. Chowdhury, J. Zielonka, B. Kalyanaraman, R.C. Hartley, M.P. Murphy, N. G. Avadhani, Mitochondria-targeted paraquat and metformin mediate ROS production to induce multiple pathways of retrograde signaling: a dose-dependent phenomenon, Redox Biol. 36 (2020), 101606.

[49] D.L. Juárez-Flores, M. Ezquerra, Ï. Gonzàlez-Casacuberta, A. Ormazabal, C. Morén, E. Tolosa, et al., Disrupted mitochondrial and metabolic plasticity underlie comorbidity between age-related and degenerative disorders as Parkinson disease and type 2 diabetes mellitus, Antioxidants 9 (2020).

[50] W.H. Tang, J. Stitham, S. Gleim, C. Di Febbo, E. Porreca, C. Fava, et al., Glucose and collagen regulate human platelet activity through aldose reductase induction of thromboxane, J. Clin. Invest. 121 (2011) 4462–4476.

[51] Q.L. Nguyen, C. Corey, P. White, A. Watson, M.T. Gladwin, M.A. Simon, et al., Platelets from pulmonary hypertension patients show increased mitochondrial reserve capacity, JCI Insight 2 (2017), e91415.

[52] S. Ravi, B. Chacko, H. Sawada, P.A. Kramer, M.S. Johnson, G.A. Benavides, et al., Metabolic plasticity in resting and thrombin activated platelets, PLoS One 10 (2015), e0123957.

[53] J. Nielsen, Systems biology of metabolism, Annu. Rev. Biochem. 86 (2017) 245–275.

[54] S. Dröse, A. Stepanova, A. Galkin, Ischemic A/D transition of mitochondrial complex I and its role in ROS generation, Biochim. Biophys. Acta 1857 (2016) 946–957.

[55] A.D. Vinogradov, V.G. Grivennikova, Oxidation of NADH and ROS production by respiratory complex I, Biochim. Biophys. Acta 1857 (2016) 863–871.

[56] A.J. Covarrubias, R. Perrone, A. Grozio, E. Verdin, NAD metabolism and its roles in cellular processes during ageing, Nat. Rev. Mol. Cell Biol. 22 (2021) 119–141.

[57] B. Glancy, D.A. Kane, A.N. Kavazis, M.L. Goodwin, W.T. Willis, L.B. Gladden, Mitochondrial lactate metabolism: history and implications for exercise and disease, J. Physiol. 599 (2021) 863–888.

[58] G. Karamanlidis, C.F. Lee, L. Garcia-Menendez, S.C. Kolwicz Jr., W. Suthammarak, G. Gong, et al., Mitochondrial complex I deficiency increases protein acetylation and accelerates heart failure, Cell Metabol. 18 (2013) 239–250.

[59] N. Diguet, S.A.J. Trammell, C. Tannous, R. Deloux, J. Piquereau, N. Mougenot, et al., Nicotinamide riboside preserves cardiac function in a mouse model of dilated cardiomyopathy, Circulation 137 (2018) 2256–2273.

[60] M.J. George, J. Bynum, P. Nair, A.P. Cap, C.E. Wade, C.S. Cox Jr., et al., Platelet biomechanics, platelet bioenergetics, and applications to clinical practice and translational research, Platelets 29 (2018) 431–439.

Abbreviation

T2DM: type 2 diabetes mellitus

LST: late stent thrombosis
PCI: percutaneous coronary interventions
OXPHOS: oxidative phosphorylation
CI: complex I
PRP: platelet rich plasma
OCR: oxygen consumption rate

ECAR: extracellular acidification rate
OPLS-DA: orthogonal partial least-squares discriminate analysis
FDR: false discovery rate
TCA: tricarboxylic acid
PPP: pentose phosphate pathway
mtROS: mitochondrial reactive oxygen species